Biointerface Research in Applied Chemistry
Open-Access Journal (ISSN: 2069-5837)

Article
Volume 16, Issue 4, 2026, 110
https://https://doi.org/10.33263/BRIAC164.110

Computational Analysis of Carotenoids Targeting Fibroblast Growth Factor (bFGF) in Comparison with Anti-Angiogenic Drug

Maysaa Alakbaree [1,*], Ali Abdulqader [1], Faisal Ali [2,3]

[1] Department of Bioinformatics, College of Biomedical Informatics, University of Information Technology and Communications (UoITC), Baghdad, Iraq; maysaa.ahmed-bic@uoitc.edu.iq (M.A.); ali.abdulkader-bic@uoitc.edu.iq (A.A.);
[2] Department of Clinical Nutrition and Dietetics, Faculty of Medicine and Health Sciences, Sanaa University, Sanaa, Yemen; sshrmany@yahoo.co.uk, F-al-shormany@su.edu.ye (F.A.);
[3] Research Advisor in Nan Yang Academy of Sciences (NAS), Singapore, Singapore
* Correspondence: maysaa.ahmed-bic@uoitc.edu.iq;

Received: 9.03.2026; Accepted: 29.05.2026; Published: 15.08.2026

Abstract: Dietary chemical carotenoids are predominantly found in colored foods and consumed worldwide. Carotenoids, whether natural or as supplements, have been shown to possess beneficial health effects, including antioxidant, anti-inflammatory, and anticancer properties; however, their effects on bFGF-mediated angiogenesis and their possible binding to bFGF are unknown. This study investigates the anti-angiogenic activity of some carotenoid substances compared to the authorized anti-angiogenic medicine (regorafenib) using an *in silico* approach. Key aspects, such as binding affinity, stability, and structural parameters, were evaluated using molecular docking and molecular dynamics simulations (MDS). Additionally, the OSIRIS tool was applied to assess toxicity risk and drug-likeness properties. Docking analysis showed that β-carotene bound strongly to bFGF (-7.5 kcal/mol), comparable to regorafenib (-7.6 kcal/mol), while zeaxanthin displayed moderate affinity (-6.6 kcal/mol), while lutein (-4.4 kcal/mol) and lycopene (-4.1 kcal/mol) exhibited weaker binding. Duplicate MDS confirmed that all carotenoid-bFGF complexes remained structurally stable, exhibiting low root mean square deviation (RMSD)/root mean square fluctuation (RMSF) values, stable radius of gyration (Rg), solvent accessible surface area (SASA), and hydrogen bond numbers similar to or higher than those of regorafenib. OSIRIS property explorer predicted a favorable safety profile for all carotenoids, with zeaxanthin and lutein showing comparatively better drug-likeness. Overall, carotenoids displayed low predicted toxicity and represented promising natural scaffolds for further investigations. These findings are based on computational analysis and require further experimental validation.

Keywords: Carotenoids; antiangiogenic activity; bFGF; regorafenib; molecular docking; molecular dynamics simulation; toxicity prediction.

© 2026 by the authors. This article is an open-access article distributed under the terms and conditions of the Creative Commons Attribution (CC BY) license (https://creativecommons.org/licenses/by/4.0/), which permits unrestricted use, distribution, and reproduction in any medium, provided the original work is properly cited. The authors retain copyright of their work, and no permission is required from the authors or the publisher to reuse or distribute this article, as long as proper attribution is given to the original source.

1. Introduction

Angiogenesis is the primary process of forming new blood vessels and plays a crucial role in both pathological and biological conditions [1]. It is slightly regulated by pro- and anti-angiogenesis factors, such as vascular endothelial growth factor (VEGF), platelet-derived

growth factor (PDGF), and angiostatin [1], which is critical for human development, invasion, and metastasis [2]. Discrepancies in the secretion levels of these proteins influence the angiogenesis process, leading to numerous clinical complications, including cancer, diabetic retinopathy, cardiovascular disorders, and impaired wound healing [3]. bFGF is a pro-angiogenic ligand that can alter vascular endothelial cell metabolism by upregulating hexokinase 2(HK2), which regulates the glycolytic process and promotes angiogenesis [4]. When bFGF binds to FGFRs, it activates downstream signaling pathways, including the PLCγ/IP3/$Ca2^{+}$ pathway [5]. This route activates protein kinase C (PKC), a key regulator of angiogenesis [5]. Tumor angiogenesis has been closely related to dysregulated bFGF signaling [3], such as adrenocortical carcinoma [5] and lung cancer [6]. bFGF was chosen as a docking target because it is a significant pro-angiogenic growth factor that directly influences endothelial cell proliferation, migration, and angiogenesis [6]. Because bFGF is a therapeutic target for many cancer treatments, such as radiation, chemotherapy, and immunotherapy [7], there is a need for a natural compound that can also target bFGF. Although a substantial amount of research has been committed to anti-cancer therapies that combat these incurable and fatal diseases, none of them has shown consistent clinical effectiveness. The purpose of this study is to investigate the potential regulatory effects of carotenoids on bFGF protein using bioinformatics tools. Cancer is a leading health problem due to high mortality and morbidity worldwide. Researchers and doctors offer other interventions to prevent cancer progression [8]. Several cancer treatments were reported by the National Cancer Institute (NCI), covering radiotherapy, immunotherapy, chemotherapy, hormone therapy, stem cell therapy, and nuclear medicine, but with progression, cancer cells can develop drug resistance [8]. Hence, a new treatment approach should be discovered, like the natural product approach. Regorafenib is considered an inhibitor of numerous kinases that promote the development of tumors as well as angiogenesis, covering vascular endothelial growth factor (VEGF), platelet-derived growth factor receptor (PDGFR), fibroblast growth factor receptor (FGFR), and pigmented epithelium-derived factor (PEDF). In typical pharmaceutical use, regorafenib is a multikinase that targets many receptor tyrosine kinases, including hence, indirectly influencing bFGF-mediated signaling pathways, rather than directly blocking bFGF [9]. Regorafenib can treat different kinds of malignancies, like prostate cancer and lung cancer, by blocking the pathways of tumor development. Further, it may address the targets involved in angiogenesis control and tumor stroma [10]. There are two main types of carotenoids: carotenes and xanthophylls. α- and β-carotene are from carrots, and lycopene is found in tomatoes [11]. These are only hydrocarbons. Xanthophylls are carotenoids that contain oxygen and additional functional groups such as alcohol, carbonyl, or other groups. Some of the xanthophylls include lutein, zeaxanthin, and α- and β-cryptoxanthin. They are powerful antioxidant compounds that protect cells from oxidative damage and aging [12].

Carotenoids represent various pigments found abundantly in fruits and vegetables [13]. These phytochemicals have been given special attention for their health benefits and biological activities [14]. Carotenoids' ability to stop angiogenesis plays a significant role in controlling cancer progression [15].

Previous studies demonstrated that carotenoids exhibit antioxidant, anti-inflammatory, and antiglycation effects by regulating pathways including NF-κB, p38 MAPK, and AGE/RAGE signaling. These biological changes may directly contribute to anti-angiogenic action by reducing oxidative stress and inflammatory mediators [16]. Carotenoids are often insoluble and have low bioavailability [17]. This limits their therapeutic potential *in vivo*,

rendering them ineffective as viable therapeutic options [18]. Furthermore, *in vivo* research is often expensive and logistically difficult, especially when investigating various chemical combinations [19]. Therefore, the current work focused on computational methodologies to guide molecular interactions between carotenoids and bFGF, thereby improving the efficiency of drug discovery and cancer therapy development, thereby addressing the limited availability of such studies. However, the interactions between carotenoids and bFGF are unknown.

The use of *in silico* approaches offers several beneficial strategies. Computational methods improve drug discovery efficiency by selecting prospective drug combinations, considerably reducing the time and resources required for investigation validation [20]. It also contributes to a better understanding of conditions, thereby increasing the accuracy of outcomes generated by simulation [19]. Most scholarly work continues to limit the use of both in vitro and in vivo investigations to explore the anticancer capabilities of carotenoids and their appropriate use. The limitations of these studies highlight the importance of combining computational methodologies to optimize drug discovery and therapeutic development. Furthermore, the findings of this study will assist the development of angiogenesis therapeutics using natural compounds and increase the interest in carotenoids' therapeutic potential for treating angiogenesis-related disorders.

2. Materials and Methods

2.1. Molecular docking.

2.1.1. Coordinates preparation.

Basic Fibroblast Growth Factor (bFGF, PDB ID:1BGF) was retrieved from the Protein Data Bank (PDB) at a resolution of 1.6 Å. The crystallographic water molecules were removed using the PyMOL molecular graphics system (version 3.1.1) to optimize the structure and facilitate accurate prediction of ligand-binding sites [21].

To analyze the surface topology and identify potential ligand-binding sites, the three-dimensional (3D) structure of 1BGF was uploaded to CASTp (Computed Atlas of Surface Topography of proteins) (http://sts.bioe.uic.edu/). This tool was employed to detect and characterize pockets, pocket mouth openings, and internal cavities within the protein structures [22].

Five substances were retrieved from the PubChem database (https://pubchem.ncbi.nlm.nih.gov/), Table 1, a comprehensive chemical repository that provides detailed information on molecular formula and structural properties [23]. As summarized in Table 1, the selected compounds included regorafenib (CID: 11167602), β-carotene (CID: 5280489), zeaxanthin (CID: 5280899), lutein (CID: 5281243), and lycopene (CID: 446925); the two-dimensional structures of the selected compounds are shown in Figure 1. The chemical structures were downloaded in SDF format based on data reported in the literature. Subsequently, the Online Smiles Translator (https://cactus.nci.nih.gov/translate/) was used to convert the structures into PDB format [24]. Ligand geometry optimization was performed using the Open Babel tool implemented in PyRx (version 0.8) through energy minimization to obtain stable conformations [25]. Each ligand was processed individually and used in PDB format for subsequent docking and analysis. To ensure the reliability and reproducibility of the docking results, the simulations were repeated multiple times, and the best constant-binding poses were selected for analysis.

Table 1. Detailed information on carotenoids used

Ligand names	Molecular formula	Molecular weight (g/mol)
Regorafenib	$C_{21}H_{15}ClF_4N_4O_3$	482.8
Zeaxanthin	$C_{40}H_{56}O_2$	568.9
β-Carotene	$C_{40}H_{56}$	536.9
Lutein	$C_{40}H_{56}O_2$	568.9
Lycopene	$C_{40}H_{56}$	536.9

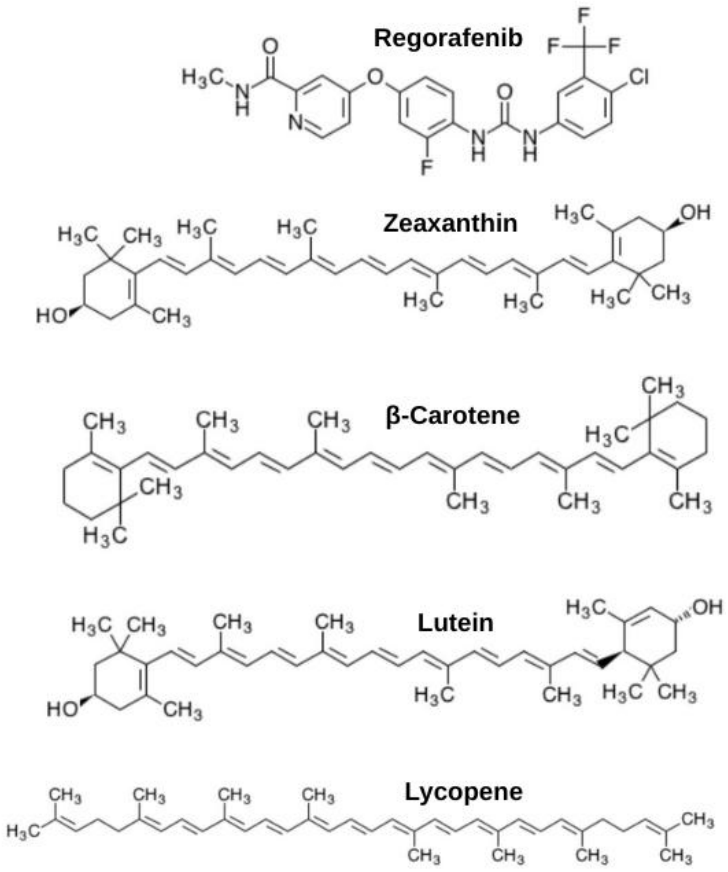

Figure 1. Two-dimensional (2D) structures of the studied compounds.

2.1.2. Molecular docking analysis and visualization.

PyRx software (v.0.8) was utilized to perform molecular docking, with the bFGF protein (1BGF) as a macromolecule and carotenoids [zeaxanthin, β-carotene, lutein, lycopene] and regorafenib as ligands [26]. PyRx software enhanced AutoDock Vina's features. In order to have a good prediction of how protein-ligands will bind correctly, the grid settings were modified [21]. Moreover, to ensure the accuracy of the docking process, all ligands provided specific coordinates for the grid center (x, y, z) and the grid size specific to them, as shown in Table 2. To generate proper conformational selection and repeatability, molecular docking was done with an exhaustiveness value of 8. For each ligand, 8 docking poses were created, and the binding pose with the highest binding affinity was chosen for further study. During the docking simulations, AutoDock Vina's default random seeds were employed. Before performing docking simulations, protein and ligand structures were created and converted to PDBQT format in the PyRX environment. PyMOL was used to generate the protein-ligand complexes by uploading the protein and each conformation with the highest affinity separately; the complexes were saved as PDB files for further analysis. To visualize the protein-ligand interactions, including non-bonded or covalently bonded interactions, BIOVIA Discovery Studio Visualizer (DSV) (v. 4.0) was used [27].

Table 2. Grid parameters for ligands docking

Ligands	Grid center points (Å)			Grid size (Å)		
	Center-x	Center-y	Center-z	Size x	Size y	Size z
Regorafenib	15.13	18.64	21.02	18.15	17.92	17.92
Zeaxanthin	18.27	14.72	21.15	18.1	25.0	20.4
β-carotene	16.28	17.04	18.55	25.0	25.0	14.0
Lutein	21.061	14.93	14.28	28.83	25.0	13.8
Lycopene	17.01	16.23	14.94	25.0	25.0	13.97

2.2. Molecular dynamics simulation (MDS).

MDS was carried out for protein-ligand complexes using the GROMACS 96 54a7 force field and GROMACS 2018.8 packages for 100 nanoseconds (ns) [28, 29]. GROMACS was installed on a computer running Ubuntu 18.04.6 LTS and equipped with an 8-core Intel Core i7-9700 [30]. Ligand topology files were created using the Automated Topology Builder (ATB) and repository (version 3.0) [31]. Each system was submerged in a cubic box with the following dimensions: box volume 3018.13 nm^3, box vectors 8.976, 11.412, and 8.233 nm, box angles 90.00 degrees, and box center (1.680, 10.069, 1.926) nm. The system was solvated using simple point-charge (SPC) water molecules, and enough sodium ions were added to balance the overall charge. In GROMACS, the genion module was used to neutralize the system by adding an appropriate quantity of sodium ions. Energy minimization was applied to the systems until the minimum energy of 1000 KJ was reached [28]. For electrostatic interactions over long distances, the particle-mesh Ewald method was employed. We used a two-visualizer ensemble technique (NVT and NPT) for 100 ps to bring all systems to equilibrium at 300K. The NVT and Parrinello-Rahman methods used Berendsen thermostats without pressure coupling. The NPT ensemble kept the pressure at 1 bar (P) [32]. We analyzed all trajectory files using the GROMACS program [29]. For the simulation trajectory analysis, the GTgrace plotting tool (https://plasma-gate.weizmann.ac.il/Grace/) was used to visualize and validate the trajectory data [29].

2.3. Toxicity risk assessment.

Osiris is a free tool that predicts the pharmacokinetic and toxicity features of drug-like molecules. It evaluates the toxicity risk for factors such as mutagenicity, tumorigenicity, irritancy, and reproductive consequences [33]. The expected results are graphically displayed using a color-code scheme, with green indicating acceptable drug-like qualities and minimal toxicity risk, and red indicating potential toxicological issues [33]. The chemical structure was uploaded in SMILES format to ensure that it is compatible with the program's automatic chemical validation mechanism. This process helps to reduce mistakes caused by inaccurate or incorrectly formatted chemical structures.

3. Results and Discussion

3.1. Molecular docking analysis.

CASTp is a computational tool that automatically identifies and measures protein surface pockets, protein mouth openings, and buried cavities, providing detailed information on lining atoms, as well as the area, volume, and circumference of pockets and cavities [34]. There are just certain residues that make up the binding site: TRP37, ILE38, GLU39, LYS73, LEU79, ILE80, HIS81, and ILE86. In addition, earlier research has shown that LYS119, ARG120, LYS125, and LYS135 are important residues involved in ligand interactions.

Docking is the process of determining the optimal orientation of a ligand within the active site of a protein receptor [35]. The PyRX software was used to bind five ligands (regorafenib, zeaxanthin, β-carotene, lutein, and lycopene) to the bFGF protein, generating protein-ligand complexes [36]. Molecular docking used the binding affinity score to assess the interaction between the molecule (ligand) and the receptors [37]. The molecular docking results suggest that the analyzed ligands showed variations in binding affinity, demonstrating their ability to bind to the target protein. For comparison, regorafenib, the control drug, has the strongest binding affinity (-7.6 Kcal/mol). The capacity of β-carotene is about the same as that of regorafenib, with a binding affinity of (-7.5 Kcal/mol). Next was zeaxanthin (-6.6 Kcal/mol), which still had a strong binding affinity. Lutein (-4.4 Kcal/mol) had a valine interaction, but its binding capability was lower, but still important. The strong affinities observed for zeaxanthin and β-carotene suggest they may be bioactive molecules warranting further investigation. However, lycopene and lutein were found to have lower binding affinities, suggesting that these ligands may exhibit limited binding capacity. These findings indicated that structural modifications influenced the process of ligand binding. Further, the additional studies indicated are required via MDS and clinical investigations to elucidate the significance of these interactions. Zeaxanthin and β-carotene have high binding affinities, indicating potential biological activity that requires further explanation. In contrast, lycopene and lutein have lower binding affinities, which may reflect an underlying limited potential for significant interactions. These observations call attention to the contribution of structural modifications to the efficiency of binding, emphasizing the necessity of further conformation with MDS. Table 3 and Figures 2-6 show the binding affinity and the different kinds of interactions formed in all complexes.

Table 3. Binding affinity analysis of various ligands against the bFGF protein

Ligand's name	Binding affinity (kcal/mol)	Interactions	Residues
Regorafenib	-7.6	Van der Waals	ASP41, ASP37, LYS86, SER87, ARG72, GLY38, ALA84
		Conventional Hydrogen Bond	GLN123, LYS77, SER85
		Carbon-Hydrogen Bond	TYR124
		Halogen	VAL40, GLN123
		Pi-Donor Hydrogen Bond	TYR124, GLU91, THR89
		Pi-Alkyl	ARG39, LEU83, TYR124
β-carotene	-7.5	Van der Waals	LYS119, GLN123, ASP37, GLY38, VAL40, ARG72, SER87, THR89, LYS77, SER85, ALA84, LEU82
		Pi-Sigma	TYR124
		Alkyl	LYS86, ARG39, LEU83, ARG81, LEU126
		Pi-Alkyl	TYR124
zeaxanthin	-6.6	Van der Waals	GLN123, LEU82, GLY38, ALA84, ARG81, ARG72, LYS119, VAL40, ASP37, SER85, LYS77, THR89
		Conventional Hydrogen Bond	SER87
		Pi-Sigma	TYR124
		Alkyl	LEU83, LYS86, ARG39
Lutein	-4.4	Van der Waals	LYS125, GLN123, ASP37, HIS50, ASP41, VAL40
		Alkyl	LYS119, LYS129, LEU126, PRO36, ARG39
		Pi-Alkyl	HIS35, TYR124
Lycopene	-4.1	Van der Waals	ASP41, ARG33
		Unfavorable Bump	GLN123
		Pi-Sigma	TYR124, HIS35
		Alkyl	ARG39, LYS119, LYS129, LEU126
		Pi-Alkyl	LEU126, HIS35

It should be highlighted that slight variations in docking scores between investigated compounds may be due to inherent constraints of molecular docking calculations and should not be regarded as definitive evidence of differences in biological potency.

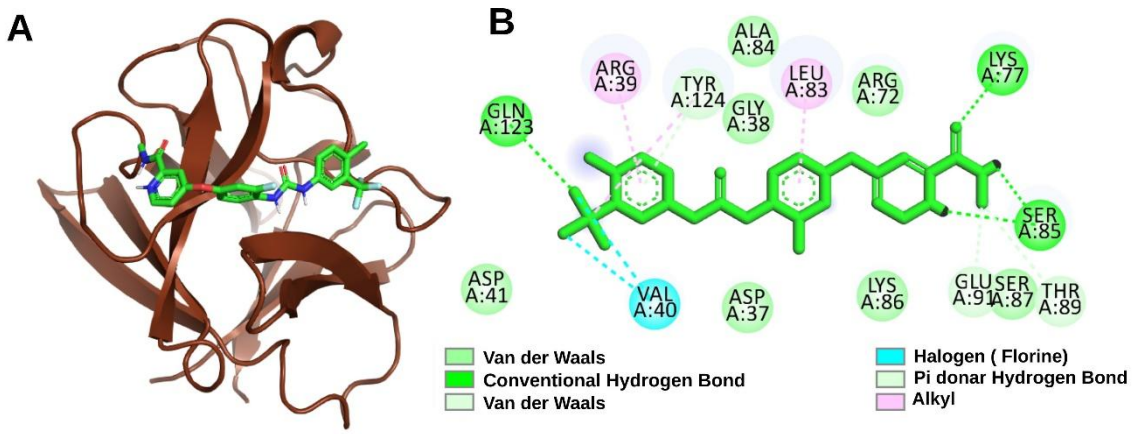

Figure 2. Docking analysis of the bFGF-regorafenib complex. **(A)** 3D structure of the docking pose showing the bFGF (brown cartoon) and ligand (green stick); **(B)** 2D interaction diagram depicting the bFGF-regorafenib interactions, including van der Waals, conventional hydrogen bonds, halogen (fluorine), pi-donor hydrogen bonds, and pi-alkyl forces. The ligand (green) is represented as sticks.

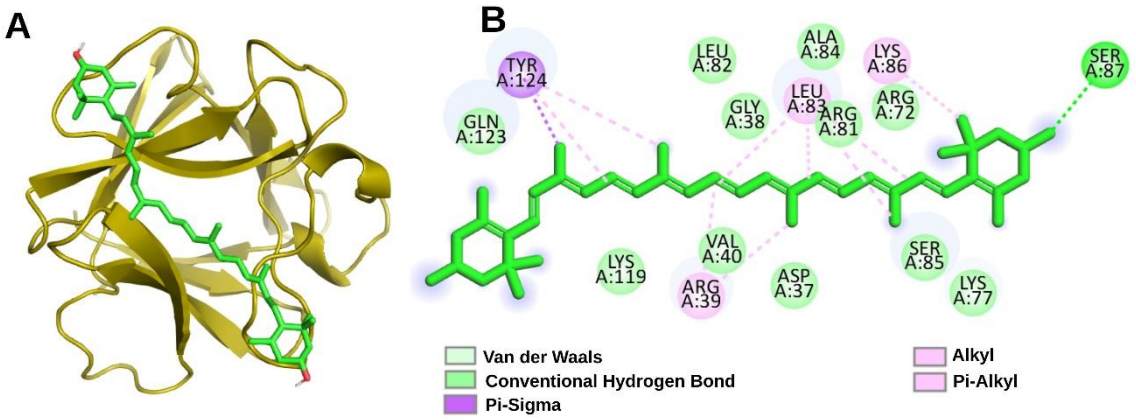

Figure 3. Docking analysis of the bFGF–zeaxanthin complex. **(A)** 3D structure of the docking pose showing the bFGF (brown cartoon) and ligand (green stick); **(B)** 2D interaction diagram depicting the bFGF-zeaxanthin interactions, including van der Waals, conventional hydrogen bonds, pi-sigma, alkyl, and pi-alkyl forces. The ligand (green) is represented as sticks.

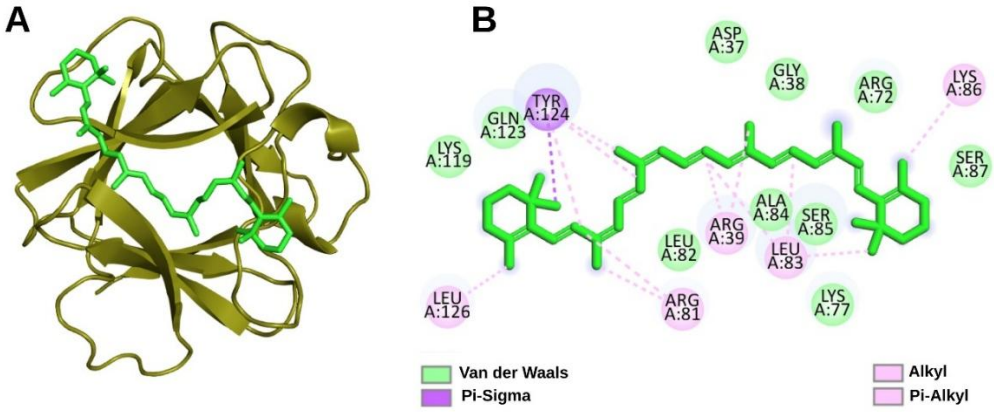

Figure 4. Docking analysis of the bFGF–*β*-carotene complex. **(A)** 3D structure of the docking pose showing the bFGF (brown cartoon) and ligand (green stick); **(B)** 2D interaction diagram depicting the bFGF-*β*-carotene interactions, including van der Waals, pi-sigma, alkyl, and pi-alkyl forces. The ligand (green) is represented as sticks.

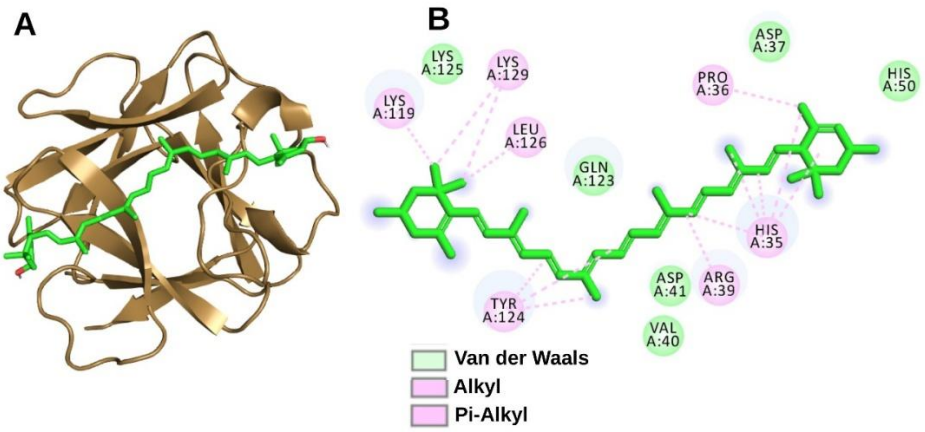

Figure 5. Docking analysis of the bFGF–lutein complex. **(A)** 3D structure of the docking pose showing the bFGF (brown cartoon) and ligand (green stick); **(B)** 2D interaction diagram depicting the bFGF-lutein interactions, van der Waals, alkyl, and pi-alkyl forces. The ligand (green) is represented as sticks.

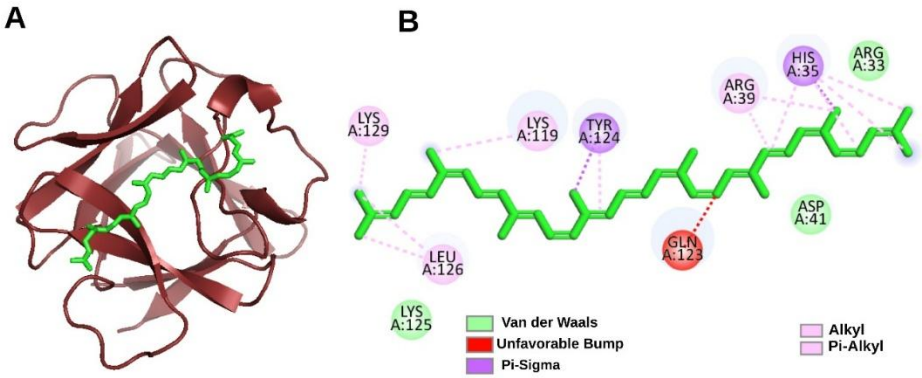

Figure 6. Docking analysis of the bFGF–lycopene complex. **(A)** 3D structure of the docking pose showing the bFGF (brown cartoon) and ligand (green stick); **(B)** 2D interaction diagram depicting the bFGF–lycopene interactions, including van der Waals, unfavorable bumps, pi-sigma, alkyl, and pi-alkyl forces. The ligand (green) is represented as sticks.

3.2. Molecular dynamics simulation (MDS).

MDS was used to assess the accuracy of docking results and the stability of protein-ligand interactions in an artificial environment [32]. Its highly successful technology is commonly employed in drug development [38]. The primary advantage of MDS is that it clearly accounts for entropic effects and structural flexibility, providing extensive information on how proteins interact with drugs or ligands and on protein dynamics [39]. It also captures receptor-ligand interactions in real time by showing how ligand binding changes over time, even as its structure changes [32]. Molecular docking illustrates only one manner in which the ligand-protein complex can fit together [32]. We performed a 100 ns MDS of bFGF complexes to better understand how they bind to one another, including the reference molecule.

3.3. Post-trajectory analysis.

3.3.1. Root mean square deviation (RMSD).

Complexes' stability was analyzed according to the RMSD after 100 ns MDS. The RMSD analysis was performed simultaneously on the ligands and the protein backbone atoms. The bFGF-carotenoid complexes exhibit more significant stability than the bFGF-regorafenib complex. The value of the RMSD should range from 0.01 to 0.35 nm [32]. The RMSD study

revealed that all complexes were highly stable over 100 ns MDS with average values ranging from 0.11 to 0.14 nm. Initial fluctuations were seen during the first (10-20) ns of the simulation's early stages, which indicated system equilibration. After which, trajectories gradually stabilized and maintained a relatively constant RMSD profile until the end of the simulation period, indicating time-dependent convergence behavior. Among the analyzed systems, the bFGF-regorafenib had the highest average RMSD value (0.14 nm) and larger fluctuations, notably between 60 and 80 ns. Carotenoid complexes with lower RMSD values, such as bFGF-zeaxanthin (0.11 nm), bFGF- β-carotene (0.12 nm), bFGF-lycopene (0.12 nm), and bFGF- lutein (0.13 nm), indicate reliable protein-ligand interactions throughout simulations; see Table 4 and Figure 7. All carotenoids also showed low deviations, indicating greater and more stable binding to bFGF than regorafenib. It subsequently demonstrated that complexes are rigid.

Table 4. RMSD values of the bFGF-carotenoid complexes.

Complexes	Average RMSD value (nm)
bFGF-regorafenib	0.14
bFGF-zeaxanthin	0.11
bFGF-β-carotene	0.12
bFGF-lutein	0.13
bFGF-lycopene	0.12

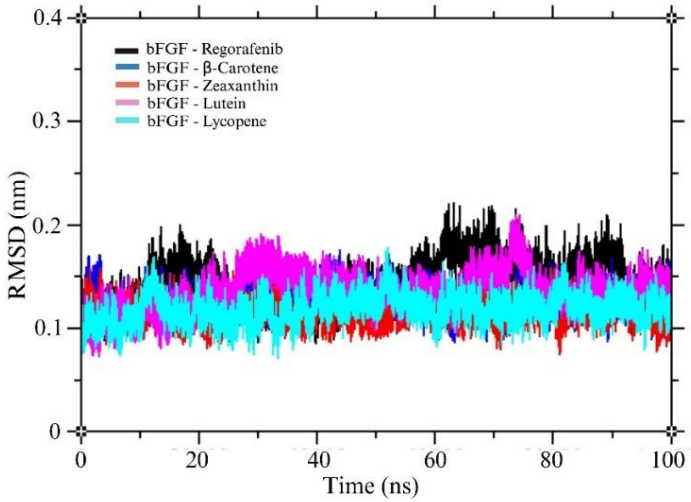

Figure 7. Time evolution of RMSD (nm) for bFGF in complex with different ligands over 100 MDS. The plot compares the structural stability of bFGF when bound to regorafenib (black), β-carotene (blue), zeaxanthin (red), lutein (magenta), and lycopene (cyan).

3.3.2. Radius of gyration (Rg).

Rg is a metric commonly used to assess the stability of complex biological systems along MD trajectories [32] by estimating the structural compactness of biomolecules. Following the MDS, the stability of the complexes was evaluated to determine whether they maintain a folded or unfolded conformation. Minor shifts were observed during the first 0-10 ns equilibration period, but the complex maintained very stable Rg trajectories for the remainder of the simulations. The average Rg values for protein-ligand complexes were comparable, ranging between [1.34 and 1.35] nm, with a minimal value of about 0.01 nm. This shows that ligand binding has minimal influence on the protein's overall compactness and structural stability. Because Rg represents the protein's compactness and flexibility, these identical results indicate that none of the ligands appreciably alter its conformation.

Regorafenib (i.e., the reference ligand) had an Rg of 1.35, which is similar to that of lycopene and lutein. If the Rg remained generally stable during the MDS, it was considered adequately folded; otherwise, it was considered unfolded [32]. We can conclude that all complexes behaved identically, with no significant variation, and that all Rg values were consistent with measurements against the reference. Therefore, we infer that these compounds are well superposed and have a high level of stability (see Table 5 and Figure 8).

Table 5. The average values of Rg (nm) in the bFGF-carotenoid complexes

Complexes	Average value of R_g
bFGF-regorafenib	1.35
bFGF-zeaxanthin	1.34
bFGF-*β*-carotene	1.34
bFGF-lutein	1.35
bFGF-lycopene	1.35

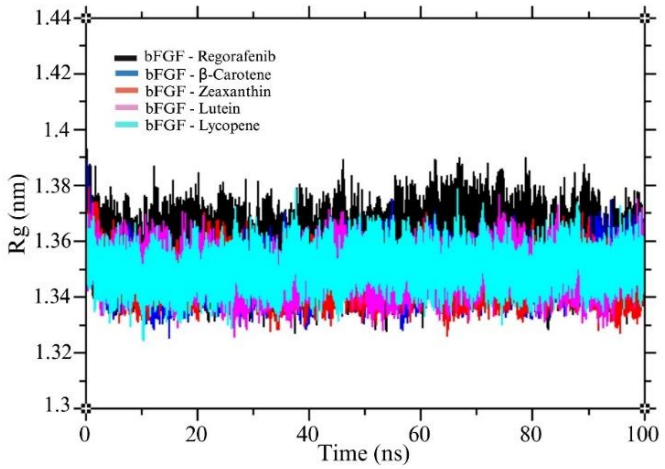

Figure 8. Rg in complex with various ligands over 100 ns MDS. The plot compares the structural compactness of bFGF when bound to regorafenib (black), *β*-carotene (blue), zeaxanthin (red), lutein (magenta), and lycopene (cyan).

3.3.3. RMSF analysis.

RMSF is a useful parameter for analyzing local fluctuations of protein chain residues and ligand atoms under specific temperature and pressure conditions [39]. The RMSF plot provides a standard representation of residues that have undergone significant changes during MDS [21]. Higher RMSF values indicate greater flexibility and the chance of local conformation changes, whereas lower RMSF values reflect more flexibility and stiffness [21]. Regorafenib exhibited significant structural fluctuations, particularly spanning amino acid residues (35-40), (118-124), and (129-139). A pronounced peak at residue 130 indicated increased local flexibility and might even change shape. All carotenoid bond complexes exhibited reduced fluctuations, indicating that the bFGF-carotenoid complexes remain structurally stable. The structures of zeaxanthin and lycopene showed marked similarity at 0.7 nm. This indicates substantial stabilizing effects. In contrast, *β*-carotene and lutein contributed to structural stability while allowing a modest degree of flexibility, which may facilitate functional adjustments in bFGF without inducing excessive rigidity.

Overall, RMSF analysis revealed that the bFGF-regorafenib complex exhibited higher flexibility (0.09 nm) compared with carotenoid-bound complexes, which showed lower RMSF values (0.07-0.08 nm), as presented in Table 6 and Figure 9. These findings indicate that all carotenoids maintain bFGF's structural stability more effectively than regorafenib, thereby

preventing excessive flexibility that could compromise protein function. The enhanced structural stability observed in carotenoid-bound complexes suggests their potential utility as natural alternatives or complementary agents in cancer therapy [40].

Table 6. Average RMSF (nm) values of bFGF in complex with different carotenoids.

Complexes	Average RMSF value (nm)
bFGF-regorafenib	0.09
bFGF-zeaxanthin	0.07
bFGF-*β*-carotene	0.08
bFGF-lutein	0.08
bFGF-lycopene	0.07

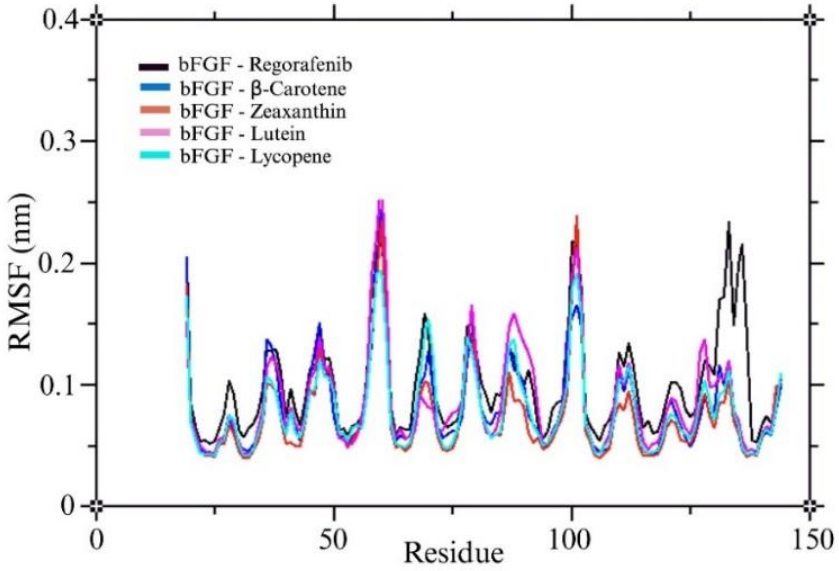

Figure 9. RMSF analysis of bFGF compared with *β*-carotene (blue), zeaxanthin (red), lutein (magenta), and lycopene (cyan) in comparison to regorafenib (black) over 100 ns.

3.3.4. Hydrogen bonds.

Hydrogen bonds have an important role in molecular recognition and protein structural stability [39]. Between 10 and 40 ns, the complexes exhibited consistent total hydrogen bond counts, ranging from 75 to 95 interactions. Rapid rises and declines were observed throughout the mid-simulation period (40-70 ns), notably in the bFGF-regorafenib complex, which fluctuated more than the carotenoid bond systems. No sustained drop in hydrogen bond number was seen. During the last (70-100) ns time frame, the carotenoid complexes, notably bFGF-lycopene and bFGF-lutein, showed rather hydrogen-bond distributions, with frequent increases exceeding about 100 interaction points. Table 7 and Figure 10 illustrate the total number of hydrogen bonds formed between bFGF and regorafenib, as well as between bFGF and *β*-carotene, zeaxanthin, lutein, and lycopene over a 100 ns simulation period. Regorafenib, a well-known anti-angiogenesis medicine [1], has an average of 84 hydrogen bonds, while carotenoids have slightly higher averages of 85 and 86. Despite these negligible differences, the general trend within the variation is similar across all compounds, with hydrogen-bonded values being largely clustered between 84 and 86. This indicates that comparable and slightly hydrogen-bonded numbers were observed for the carotenoid-bFGF complexes relative to the bFGF-regorafenib complex. Overall, the hydrogen bond analysis indicated that all hydrogen bonds in complexes had similar interaction networks and overall structural stability during the MDS.

Table 7. Total number of H-bonds in bFGF-carotenoid complexes.

Complexes	Average value of H-bond
bFGF-regorafenib	84
bFGF-zeaxanthin	86
bFGF-*β*-carotene	85
bFGF-lutein	86
bFGF-lycopene	86

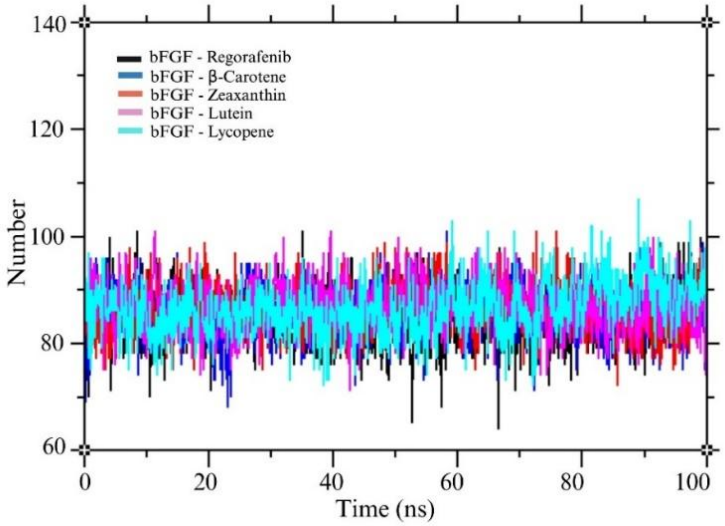

Figure 10. Total number of H-bond analyses. H-bonds formed in bFGF-carotenoid complexes throughout a 100 ns MDS. Regorafenib (black), *β*-carotene (blue), zeaxanthin (red), lutein (magenta), and lycopene (cyan).

3.3.5. SASA analysis.

The SASA analysis quantifies the solvent-accessible surface area of a protein, which can influence various biophysical properties [41]. SASA influences a variety of biophysical parameters and is critical for protein folding and stability because it classifies amino acid residues as buried or exposed, thereby affecting their interactions and function. Such a parameter is useful for evaluating the compactness of backbone atom treatment. SASA fluctuations over time indicate complexes undergoing folding and unfolding, with lower SASA scores suggesting greater structural compactness [41]. The SASA values indicate small differences in the compactness of the bFGF protein upon complexation with various carotenoids. Between 10 and 50 ns, all complexes exhibited relatively stable SASA values, with only minor fluctuations. During the following simulation period (50-100 ns), the complexes maintained a highly stable SASA profile, with no significant increases or decreases. bFGF-regorafenib is the reference and has a good SASA value (72 nm²), indicating a relatively more expanded conformation. The bFGF-*β*-carotene and bFGF-lutein complexes presented the lowest SASA values (70 nm²), denoting a more compact structural fold. Meanwhile, the bFGF-zeaxanthin and bFGF-lycopene complexes obtained a SASA value of 71 nm² (Table 8 and Figure 11). These subtle differences imply that different carotenoids influence the protein's structural conformation to a minor extent. It was observed that despite such a difference, carotenoids can bind in bFGF's hydrophobic pocket without causing major distortions, as supported by their narrow SASA range of (70.0–72.0) nm². Their binding does not significantly affect the compactness estimation of the structure, and variations are unlikely to reflect a meaningful impact on changes in protein stability throughout the complexes. The investigation of SASA and hydrogen bonding further confirms that the small molecules are stably bound to the protein.

Table 8. Average SASA (nm^2) values for bFGF in complexes with different carotenoids.

Complexes	SASA (nm^2)
bFGF-regorafenib	72
bFGF-zeaxanthin	71
bFGF-*β*-carotene	70
bFGF-lutein	70
bFGF-lycopene	71

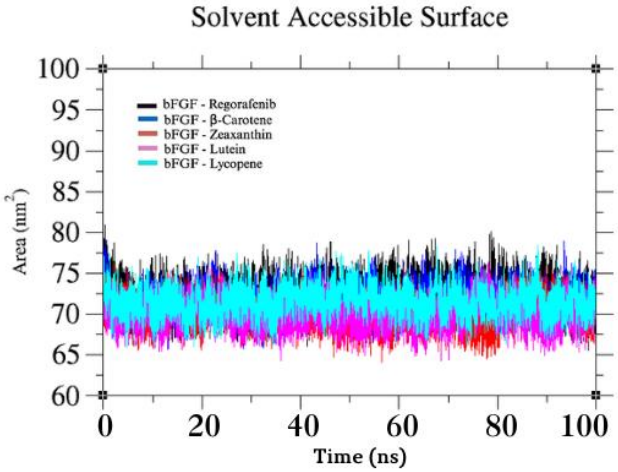

Figure 11. SASA analysis of bFGF bound with *β*-carotene (blue), zeaxanthin (red), lutein (magenta), and lycopene (cyan) in comparison to regorafenib (black) over a 100 ns simulation.

Generally, the MDS analysis enables us to understand better the conformational behavior of the bFGF protein in the presence of regorafenib and carotenoid molecules. The findings (Table 9) emphasize that carotenoid complexes maintained stable interactions throughout the simulations, with stability patterns similar to those reported for the regorafenib complex. Additional experimental validation may be necessary to validate the biological stability and activity of the selected compounds, which may act as antiangiogenic compounds. It also provides a better platform to support future discoveries and the development of new substances for angiogenesis.

Table 9. Summary of average values from the MDS results.

Complexes	RMSD (nm)	Rg (nm)	RMSF (nm)	H-bonds (number)	SASA (nm^2)
bFGF-regorafenib	0.14	1.35	0.09	84	72
bFGF-zeaxanthin	0.11	1.34	0.07	86	71
bFGF-*β*-carotene	0.12	1.34	0.08	85	70
bFGF-lutein	0.13	1.35	0.08	86	70
bFGF-lycopene	0.12	1.35	0.07	86	71

3.4. Toxicity risk assessment.

To identify significant factors such as toxicity, the OSIRIS prediction tool was employed [42]. The toxicity profiles of the selected carotenoids were compared with that of the reference molecule. The evaluated parameters are summarized in Table 10 and Figure 12. The *in silico* assessment indicated that the reference molecule (regorafenib) and the chosen carotenoids (zeaxanthin, β-carotene, lutein, and lycopene) were predicted to be non-mutagenic, non-tumorigenic, and non-reproductively toxic, with only lutein showing a potential irritant effect. These suggested a generally favorable safety profile, based on OSIRIS fragment-based toxicity prediction, as therapeutic effectiveness is closely dependent on drug safety [43].

Notable variations were noted in key physicochemical parameters relevant to pharmacokinetics, particularly molecular weight and lipophilicity. All evaluated carotenoids

had molecular weights above 500 Da, which may limit their oral bioavailability. However, several approved drugs exceed this threshold, and natural compounds have been reported to retain permeability up to approximately 700 Da, indicating that molecular weight does not preclude therapeutic potential [44]. Regorafenib exhibited moderate calculated logarithm of octanol-water partition coefficient lipophilicity (cLogP=4.24), whereas all carotenoids showed excessive lipophilicity (12.0-16.3), exceeding the optimal range associated with good absorption. Consistent with this, all carotenoids displayed moderate predicted aqueous solubility (LogS = -6.54 to -7.6). Regorafenib also showed substantially higher topological polar surface area (TPSA=92.35 $Å^2$) compared with zeaxanthin and lutein (40.46 $Å^2$), while β-carotene and lycopene exhibited zero TPSA, reflecting their highly nonpolar nature.

Drug-likeness analysis revealed positive values for zeaxanthin and lutein (0.35), whereas regorafenib, β-carotene, and lycopene displayed negative values. Integration of these parameters into the drug score showed that regorafenib had the highest overall score (0.23), followed by zeaxanthin and lutein (0.15), with β-carotene and lycopene having the lowest scores. Among carotenoids, zeaxanthin and lutein showed more favorable drug-likeness, making them suitable starting scaffolds for further optimization, and their favorable *in silico* toxicity profiles are consistent with a previous report describing their preventive and protective health effects. Despite a hopeful computational finding, carotenoids may pose pharmaceutical challenges due to their high lipophilicity, limited water solubility, and potentially low bioavailability. Furthermore, additional experimental studies are needed to confirm current computational findings.

Table 10. Molecular properties prediction and toxicity profile of carotenoids in comparison with the reference drug (regorafenib).

Categories properties	Regorafenib	Zeaxanthin	*β*-carotene	Lutein	Lycopene
Mutagenic	No	No	No	No	No
Tumorigenic	No	No	No	No	No
Irritant	No	No	No	Yes	No
Reproductive effect	No	No	No	No	No
cLogP	4.24	12.17	13.87	12.0	16.3
Solubility	-7.0	-6.54	-7.33	-6.57	-7.6
MW	482	568	536	568	540
TPSA	92.35	40.46	0.0	40.46	0.0
Drug-likeness	-5.02	0.35	-3.35	0.35	-4.56
Drug score	0.18	0.15	0.1	0.15	0.06

Figure 12. *In silico* evaluation of toxicity risk and drug-likeness parameters of the investigated carotenoids in comparison with the reference drug (regorafenib).

The current study used the OSIRIS property explorer as a preliminary toxicity prediction tool; however, future studies may use an additional ADMET platform for more in-depth pharmacokinetic and toxicity evaluation.

4. Conclusion

The present *in silico* study indicated that selected carotenoids form stable complexes with bFGF, suggesting their potential role in anti-angiogenic activity. *β*-carotene showed binding affinity comparable to the reference drug regorafenib, while zeaxanthin exhibited the most balanced profile in terms of binding affinity and drug-likeness. Lutein, despite weaker binding, maintained favorable interaction and acceptable drug-likeness characteristics. In addition, toxicity predictions indicated a generally safe profile for all investigated carotenoids. The findings of this study demonstrate the potential of carotenoids as natural scaffolds for future anti-angiogenic drug development targeting bFGF. However, the present work is based on computational predictions; further experimental pharmacological studies are required to validate their biological activity and therapeutic potential. Overall, this study provides a computational framework that may guide future experimental investigations and the development of new anti-angiogenic agents.

Author Contributions

Conceptualization, M.A. and A.A.; methodology, M.A. and A.A.; software, M.A.; validation, M.A., A.A., and F.A.; formal analysis, M.A. and A.A.; investigation, F.A.; resources, A.A.; writing—original draft preparation, M.A. and A.A.; writing—review and editing, A.A. and F.A.; supervision, F.A.; project administration, M.A. All authors have read and agreed to the published version of the manuscript.

Institutional Review Board Statement

Not applicable.

Informed Consent Statement

Not applicable.

Data Availability Statement

Data supporting the findings of this study are available upon reasonable request from the corresponding author.

Funding

This research received no external funding.

Acknowledgments

The authors would like to thank the Department of Bioinformatics, College of Biomedical Informatics, University of Information Technology and Communications (UoITC), Baghdad, Iraq, for its support during this research.

Conflicts of Interest

The authors declare no conflict of interest.

Role of Funders

Not applicable.

Abbreviations

The following abbreviations are used in this manuscript:

Abbreviation	Definition
VEGF	Vascular Endothelial Growth Factor
PDGF	Platelet-derived Growth Factor
bFGF	Basic Fibroblast Growth Factor
NCI	National Cancer Institute
PDGFR	Platelet-derived Growth Factor Receptor
FGER	Fibroblast Growth Factor Receptor
PEDF	Pigmented Epithelium-derived Factor
PDB	Protein Data Bank
CASTp	Computed Atlas of Surface Topography of Proteins
DSV	Discovery Studio Visualizer
ATB	Automated Topology Builder
ps	Picosecond
ns	Nanosecond
RMSD	Root Mean Square Deviation
RMSF	Root Mean Square Fluctuation
Rg	Radius of Gyration
SASA	Solvent Accessible Surface Area
TPSA	Topological Polar Surface Area
MW	Molecular Weight

References

1. Rallis, K.S. Targeting Angiogenesis in Cancer Therapy: Lessons Learned and Paths Forward. *Expert Rev. Anticancer Ther.* **2026**, 26, 437-450, https://doi.org/10.1080/14737140.2025.2599893
2. Ivanov, A.N.; Chabbarov, Y.R. Mechanisms of Physiological Angiogenesis. *J. Evol. Biochem. Physiol.* **2023**, *59*, 914–929, https://doi.org/10.1134/S0022093023030237
3. Liu, Z.L.; Chen, H.H.; Zheng, L.L.; Sun, L.P.; Shi, L. Angiogenic Signaling Pathways and Anti-Angiogenic Therapy for Cancer. *Signal Transduct. Target. Ther.* **2023**, *8*, 198, https://doi.org/10.1038/s41392-023-01460-1
4. Liu, X.; Hu, J.; Gan, W.; Liu, F.; Zhong, B. Molecular Mechanisms of Juvenile Nasopharyngeal Angiofibroma : A Narrative Review. *Curr. Oncol.* 2026, 33-147, https://doi.org/10.3390/curroncol33030147
5. Ardizzone, A.; Bova, V.; Casili, G.; Repici, A.; Lanza, M.; Giuffrida, R.; Colarossi, C.; Mare, M.; Cuzzocrea, S.; Esposito, E.; et al. Role of Basic Fibroblast Growth Factor in Cancer: Biological Activity, Targeted Therapies, and Prognostic Value. *Cells* **2023**, *12*, 1–29, https://doi.org/10.3390/cells12071002.
6. Peng, M.; Deng, J.; Li, X. Clinical Advances and Challenges in Targeting FGF / FGFR Signaling in Lung Cancer. *Mol* cancer, **2024**, 23, 256, https://doi.org/10.1186/s12943-024-02167-9
7. Li, C.Y.; Kuang, K.L.; Du, J.R.; Eymin, B.; Jia, T. Far beyond Anti-Angiogenesis: Benefits for Anti-BasicFGF Therapy in Cancer. *Biochim. Biophys. Acta - Mol. Cell Res.* **2022**, *1869*, 119253, https://doi.org/10.1016/j.bbamcr.2022.119253
8. Fawwaz, M.; Pratama, M.; Hasrawati, A.; Sukmawati; Widiastuti, H.; Rahmawati; Abidin, Z. Total Carotenoids, Antioxidant and Anticancer Effect of Penaeus Monodon Shells Extract. *Biointerface Res. Appl. Chem.* **2021**, *11*, 11293–11302, https://doi.org/10.33263/BRIAC114.1129311302
9. Han, J.; Liang, W.; Li, K. Unveiling the Tumor Microenvironment in Colorectal Cancer Therapeutic Resistance. *Front. Cell Dev. Biol.* **2026**, *13*, 1753180, https://doi.org/10.3389/fcell.2025.1753180
10. Elamarthi, P. Regorafenib: A Narrative Drug Review. *Cancer Res. Stat. Treat.* **2022**, *5*, 293–301, https://doi.org/10.4103/crst.crst_110_22.

11. Dos Santos, P.M.; Scaglia, B. A Enzyme-Assisted Carotenoid Extraction from Residual Biomass: The Case of Lycopene, Beta-Carotene, and Astaxanthin. *Waste and Biomass Valorization* **2026**, 1–17, https://doi.org/10.1007/s12649-026-03562-7
12. George, B.P.; Chandran, R.; Abrahamse, H. Role of Phytochemicals in Cancer Chemoprevention: Insights. *Antioxidants* **2021**, *10*, 1455, https://doi.org/10.3390/antiox10091455
13. Rowles, J.L.; Erdman, J.W. Carotenoids and Their Role in Cancer Prevention. *Biochim. Biophys. Acta - Mol. Cell Biol. Lipids* **2020**, *1865*, 158613, https://doi.org/10.1016/j.bbalip.2020.158613
14. Bhatt, T.; Patel, K. Carotenoids: Potent to Prevent Diseases Review. *Nat. Products Bioprospect.* **2020**, *10*, 109–117, https://doi.org/10.1007/s13659-020-00244-2
15. Albini, A.; Noonan, D.M.; Corradino, P.; Magnoni, F.; Corso, G. The Past and Future of Angiogenesis as a Target for Cancer Therapy and Prevention. *Cancer Prev. Res.* **2024**, *17*, 289–303, https://doi.org/10.1158/1940-6207.CAPR-24-0085
16. Antunes, A.; Carmo, F.; Pinto, S.; Andrade, N.; Martel, F. The Anti-Proliferative Effect of β-Carotene against a Triple-Negative Breast Cancer Cell Line Is Cancer Cell-Specific and JNK-Dependent. *PharmaNutrition* **2022**, *22*, 100320, https://doi.org/10.1016/j.phanu.2022.100320
17. Wang, B.; Fu, Y. Bioavailability of Carotenoids. In *Bioavailability of Nutraceuticals and Bioactive Compounds*; CRC Press, **2025**; pp. 177–193, https://doi.org/10.1201/9781003312741-9
18. Koklesova, L.; Liskova, A.; Samec, M.; Zhai, K.; Abotaleb, M.; Ashrafizadeh, M.; Brockmueller, A.; Shakibaei, M.; Biringer, K.; Bugos, O.; et al. Carotenoids in Cancer Metastasis—Status Quo and Outlook. *Biomolecules* **2020**, 10, 1653, https://doi.org/10.3390/biom10121653
19. Schoon, H.; Slack, E.; Pearce, M.; Ng, W.F.; Hackett, K.L. Activity Interference in Patients with Sjögren's Syndrome: A Cross-Sectional Study of 149 Patients in the UK. *Rheumatol. (United Kingdom)* **2022**, *61*, 4065–4075, https://doi.org/10.1093/rheumatology/keac053
20. Mehran, M.J.; Mohammadzadeh, S.; Bolideei, M.; Barzigar, R.; Haider, K.H.; Jadgal, N.; Bahrami, Y. Artificial Intelligence in Drug Discovery: Integrative Advances From Data to Therapeutic Innovation. *Drug Dev. Res.* **2026**, *87*, e70229, https://doi.org/10.1002/ddr.70229
21. Ghahremanian, S.; Rashidi, M.M.; Raeisi, K.; Toghraie, D. Molecular Dynamics Simulation Approach for Discovering Potential Inhibitors against SARS-CoV-2: A Structural Review. *J. Mol. Liq.* **2022**, *354*, 118901, https://doi.org/10.1016/j.molliq.2022.118901.
22. Sarkar, S.; Das, S.; Ali, M.H. In Silico Structural and Functional Characterization of the HMPV M2-1 Protein Reveals Its Potential as a Therapeutic Target. *J. Med. Chem. Ther.* **2026**, *2*, 1–11, https://doi.org/10.71193/jmct.20250008
23. Naveed, M.; Khatoon, K.; Aziz, T.; Naveed, R.; Majeed, M.N.; Salah, M.; Din, U.; Javed, T.; Khan, A.A.; Alasmari, A.F. Scrutinizing the Evidence of Anthracene Toxicity on Adrenergic Receptor Beta-2 and Its Bioremediation by Fungal Manganese Peroxidase via in Silico Approaches. *Sci. Rep.* **2025**, 15, 3795, https://doi.org/10.1038/s41598-025-85889-0
24. Jayaraman, S. Molecular Docking Analysis of Vascular Endothelial Growth Factor Receptor with Bioactive Molecules from Piper Longum as Potential Anti-Cancer Agents. *Bioinformation* **2021**, *17*, 223–228, https://doi.org/10.6026/97320630017223
25. Ayodele, O.; Sabiu, S. Integrated Bioprospection of Phenolics as Potent Modulators of Acinetobacter Baumannii Penicillin-Binding Protein 1A. *J. Chem.* **2026**, *2026*, 6663249, https://doi.org/10.1155/joch/6663249
26. Hossain, M.A.; Dewan, P.; Kawsar, S.M.A.; Dangwal, A.; Kalra, K.; Kalra, J.M.; Ashok, P.K.; Parashar, T.; Jakhmola, V.; Saha, S.; et al. Chemical Descriptors, ADMET, Molecular Docking and Molecular Dynamics Simulation of Mannopyranoside Derivatives against Smallpox Virus Proteins. *Adv. J. Chem. Sect. A* **2025**, *8*, 1–16, https://doi.org/10.48309/ajca.2025.459071.1531
27. Rahman, M.H.; Biswas, P.; Dey, D.; Hannan, M.A.; Sahabuddin, M.; Araf, Y.; Kwon, Y.; Emran, T. Bin; Ali, M.S.; Uddin, M.J. An *In silico* Identification of Potential Flavonoids against Kidney Fibrosis Targeting TGFβR-1. *Life* **2022**, *12*, 1764, https://doi.org/10.3390/life12111764
28. Cao, K.; Wang, R.; Li, R.; Xiong, X.; Liu, X. Investigation of the Interaction between Glucose-6-Phosphate Dehydrogenase and ATA-Inhibitor by Molecular Docking and Molecular Dynamics Simulation. *Int. J. Biol. Life Sci.* **2022**, *1*, 60–63, https://doi.org/10.54097/ijbls.v1i1.3575
29. Lemkul, J. From Proteins to Perturbed Hamiltonians: A Suite of Tutorials for the GROMACS-2018 Molecular Simulation Package [Article v1.0]. *Living J. Comput. Mol. Sci.* **2019**, *1*, 1–53, https://doi.org/10.33011/livecoms.1.1.5068
30. Baammi, S.; El Allali, A.; Daoud, R. Unleashing Nature's Potential: A Computational Approach to Discovering Novel VEGFR-2 Inhibitors from African Natural Compound Using Virtual Screening, ADMET Analysis, Molecular Dynamics, and MMPBSA Calculations. *Front. Mol. Biosci.* **2023**, *10*, 1–10, https://doi.org/10.3389/fmolb.2023.1227643
31. Boonyuen, U.; Jacob, B.A.C.; Wongwigkan, J.; Chamchoy, K.; Singha-art, N.; Pengsuk, N.; Songdej, D.; Adams, E.R.; Edwards, T.; Chamnanchanunt, S.; et al. Genetic Analysis and Molecular Basis of G6PD Deficiency among Malaria Patients in Thailand: Implications for Safe Use of 8-Aminoquinolines. *Malar. J.* **2024**, *23*, 1–17, https://doi.org/10.1186/s12936-024-04864-8

32. Kavitha, K.; Srikrishna, D.; Aparna, P. An Efficient One-Pot Three-Component Synthesis of 2-(4-(2-Oxo-2H-Chromen-3-Yl)Thiazol-2-Yl)-3-Arylacrylonitriles and Their Cytotoxic Activity Evaluation with Molecular Docking. *J. Saudi Chem. Soc.* **2019**, *23*, 325–337, https://doi.org/10.1016/j.jscs.2018.08.007
33. Devi, B.K.; Madhavi, K.; Rajitha, G. Synthesis , Biological Evaluation and in Silico Studies of Novel N-(4- (2- (2-Cyano-3- Isobutylphenyl) Propanamides. *Indiand j. Chem*. **2026**, *65*, 32–4. https://doi.org/10.56042/ijc.v65i1.26281
34. Meesala, S.; Nageswara, S.; Kolakota, R.; Dokka, M.K.; Giri, M.; Bada, P. In Silico Prediction of Octahydro-1H- Indole-2-Carboxamide Derivatives as Novel Acetylcholinesterase Inhibitors : A Comprehensive Computational Study. *Egypt. J. Med. Hum. Genet.* **2026**, *27*, *37*, https://doi.org/10.1186/s43042-026-00858-0
35. Vaghela, A.R. Molecular Docking in Drug Design : Basic Concepts and Application Spectrums. *Am, J, Pharmacother,Pharm, Sci*. **2026**, 1–10, https://doi.org/10.25259/AJPPS_2026_001
36. Sivaraj, C.; Anantharaman, R.; Yesudass, S. In Silico Molecular Docking Analysis of Phytochemicals from Phaseolus Vulgaris Against Cancer-Associated Target Proteins. *Silico Res. Biomed.* **2026**, 100397, https://doi.org/10.1016/j.insi.2026.100397
37. Joshi, T.; Joshi, T.; Sharma, P.; Chandra, S.; Pande, V. *Molecular Docking and Molecular Dynamics Simulation Approach to Screen Natural Compounds for Inhibition of Xanthomonas Oryzae Pv. Oryzae by Targeting Peptide Deformylase*; *J. Biomol. Stru*t. Dyn. 2020. 39, 823, 840, https://doi.org/10.1080/07391102.2020.1719200
38. Kumar, M.; Tripathi, M.K.; Kaur, P. Molecular Dynamics and Its Significance in Drug Discovery. In *Structure-Based Drug Design*; Springer, **2024**; pp. 149–175, https://doi.org/10.1007/978-3-031-69162-1_6
39. Wang, Y.; Chen, S.; Cao, Y.; Wen, X.; Fu, C.; Liang, J.; Luo, Q.; Liu, Q. Molecular Dynamics and Experimental Validation of Natural Products from Chuanxiong Rhizoma as VEGFR2 Inhibitors for NAMD Therapy. **2026**, https://doi.org/10.1021/acsomega.5c07274
40. Baeza-Morales, A.; Medina-García, M.; Martínez-Peinado, P.; Pascual-García, S.; Pujalte-Satorre, C.; López-Jaén, A.B.; Martínez-Espinosa, R.M.; Sempere-Ortells, J.M. The Antitumour Mechanisms of Carotenoids: A Comprehensive Review. *Antioxidants* **2024**, *13*, 1060, https://doi.org/10.3390/antiox13091060
41. Pal, P.; Debnath, R.; Jana, B.; Chakraborty, S. Solvent Accessible Surface Area Normalized Protein-Water Hydrogen Bonds Defines Protein Folded State Stability and Amyloid Formation. *Phys. Chem. Chem. Phys.* **2026**, 28, 4321-4332, https://doi.org/10.1039/d5cp04425a
42. Vyas, R.; Ali, A.; Lujain, F.A.; Aldosari, I.N.; Ahmed, M.; Alarcón-sánchez, M.A.; Heboyan, A.; Alarcón-sánchez, M.A. Molecular Dynamics Simulation of Polymerization Kinetics, Dimensional Stability , and in Silico Toxicity of Nextgeneration Silicone Impression Materials in Dentistry. *J. Mater. Sci. Mater. Med.* **2025**, 36, 73, https://doi.org/10.1007/s10856-025-06944-w
43. Liu, H. Advancing ADMET Prediction through Multiscale Fragment-Aware Pretraining with MSformer -ADMET. **2025**, *26*, https://doi.org/10.1093/bib/bbaf506
44. Stegemann, S.; Moreton, C.; Svanbäck, S.; Box, K.; Motte, G.; Paudel, A. Trends in Oral Small-Molecule Drug Discovery and Product Development Based on Product Launches before and after the Rule of Five. *Drug Discov. Today* **2022**, 28, 103344, https://doi.org/10.1016/j.drudis.2022.103344

Publisher's Note & Disclaimer

The statements, opinions, and data presented in this publication are solely those of the individual author(s) and contributor(s) and do not necessarily reflect the views of the publisher and/or the editor(s). The publisher and/or the editor(s) disclaim any responsibility for the accuracy, completeness, or reliability of the content. Neither the publisher nor the editor(s) assume any legal liability for any errors, omissions, or consequences arising from the use of the information presented in this publication. Furthermore, the publisher and/or the editor(s) disclaim any liability for any injury, damage, or loss to persons or property that may result from the use of any ideas, methods, instructions, or products mentioned in the content. Readers are encouraged to independently verify any information before relying on it, and the publisher assumes no responsibility for any consequences arising from the use of materials contained in this publication.